Chapter 4

H I Shells Behind the Coalsack

A slightly modified version of this chapter has been accepted for publication in the Astrophysical Journal with the reference: McClure-Griffiths, N. M., Dickey, J. M., Gaensler, B. M., Green, A. J. 2001, ApJ, 562, in press

Abstract

We report the discovery of two new large H I shells in the direction of the Coalsack nebula. Both shells were observed with the Parkes Radio Telescope as part of the Southern Galactic Plane Survey. The largest shell, GSH 304-00-12, is at a distance of $\sim$ 1.2 kpc and has derived physical dimensions of 280 $\times$ 200 pc. The second shell, GSH 305+01-24, is at a distance of $\sim$ 2.2 kpc and has derived dimensions of 280$\times$440 pc. We present a simple numerical model to show that GSH 305+01-24 most likely formed from stellar winds in the Centaurus OB1 stellar association. There is associated radio, infrared and Hα continuum emission. Both shells are situated in the Sagittarius-Carina arm, with GSH 305+01-24 more distant. The far edge of GSH 304-00-12 is at the near side of the arm and opens into the interarm region. We find no evidence for closure at the near side of the shell and therefore describe the geometry as conical. Emission from the near side of the shell may be lost in absorption by the Coalsack Nebula.

4.1 Introduction

Most shells form from the combined effects of stellar winds and supernovae that inject large quantities of energy ($10^{51} - 10^{53}$ ergs) into the ISM. A few studies have directly identified the shell power source as an OB association (e.g. Saken et al. 1992; Brown et al. 1995). In these cases, however, standard wind blown bubble models (e.g. Weaver et al. 1977) fail to properly account for the shells' radii and expansion velocities. As noted by Oey & Massey (1995), the model typically predicts radii that are too large and expansion velocities that are too small compared to the Large Magellanic Cloud (LMC) shell population.

We here report on the identification of two large shells, GSH 304-00-12 and GSH 305+01-24, located at the edge of the nearby Sagittarius-Carina spiral arm. The Coalsack nebula lies between the Sun and the near edge of GSH 304-00-12, though it does not appear physically related to the shell. We believe that GSH 305+01-24 is associated with the Centaurus OB1 stellar association. We employ a very simple model for a wind-blown bubble to show that the shell is well explained by the cataloged stars in Cen OB1. These objects were identified in the Parkes portion of the SGPS. Observations and analysis of these data are described in Chapter 2. In § 4.2 we describe the shells morphologically and dynamically and suggest a geometry to explain their characteristics. In § 4.2.3 we explore the relationship of GSH 305+01-24 with Cen OB1

4.2 H I Shells GSH 304-0-12 and GSH 305+1-24

We here present images of a new pair of shells in the direction of the Southern Coalsack. The larger shell has an extremely large angular size of $29° \times 20°$ and is centered at $l = 303\overset{\circ}{.}9$, $b = -0\overset{\circ}{.}2$, $v = -11.5$ km s^{-1}. Following the IAU standard naming convention based on the center coordinates of the shell, we name this shell GSH 304-00-12. Velocity channel images of GSH 304-00-12 from -14.8 km s^{-1} to -7.2 km s^{-1} in intervals of

2.5 km s^{-1} are shown in Fig. 4.1. The shell is a large elliptical structure extending to $|b| \sim 10°$ in an arc that is nearly symmetric about the plane. For clarity, the shell is shown again in Fig. 4.2, a composite image that includes an H I image of the shell at $v = -12$ km s^{-1}(panel a), a latitude cut across the shell (panel b), and a velocity profile through the shell (panel c). The H I image is marked with an ellipse that traces the edge of the shell. There is a vertical line marking the position of the latitude cut and a cross-hair marking the position of the velocity profile.

The shell first appears near $v \approx -27$ km s^{-1}, embedded in the H I emission from the Sagittarius-Carina arm, where it is as an arc of length $\sim 20°$ peaked at $b \approx 9°$. Between $v = -15$ km s^{-1} and $v = -9$ km s^{-1} the size of the shell is roughly constant. At the central velocity of $v = -12$ km s^{-1} the shell is brightest on the high longitude end of the images and traces a faint arc through the low-longitude end. Towards larger velocities (i.e. towards the local gas) it decreases in angular size and finally disappears at $v \approx -4$ km s^{-1}. The caps of the shell, on both the near and far sides are not readily detected. On the near side, at $v \sim -4$ km s^{-1}, emission from the shell is obscured by absorption in the Coalsack nebula and emission from the local gas. The geometry of this shell is best described as conical. If there is emission from the far cap at $v > 30$ km s^{-1}, it is swamped by the H I emission from the Sagittarius-Carina spiral arm. As seen in Figs. 4.1 & 4.2, the emission void above the plane contains a vertical filament at $l \approx 306°$, extending from $b \approx 3\overset{\circ}{.}5$ to the top of the shell. This filament appears to correspond to the Galactic worm GW 305.5+9.4 (Koo et al. 1992).

Using the Galactic rotation model of Fich et al. (1989) and adopting the IAU standard values for the Sun's orbital velocity, $\Theta_0 = 220$ km s^{-1}, and Galactic center distance, $R_0 = 8.5$ kpc, we estimate the distance to GSH 304-00-12 from the central velocity of $v = -12$ km s^{-1}. Assuming a velocity error of ± 10 km s^{-1} to account for streaming motions (Burton 1988), we determine a distance of $D = 1.2 \pm 1.0$ kpc. At this distance the shell has physical diameters of 280 pc and 200 pc in the longitude

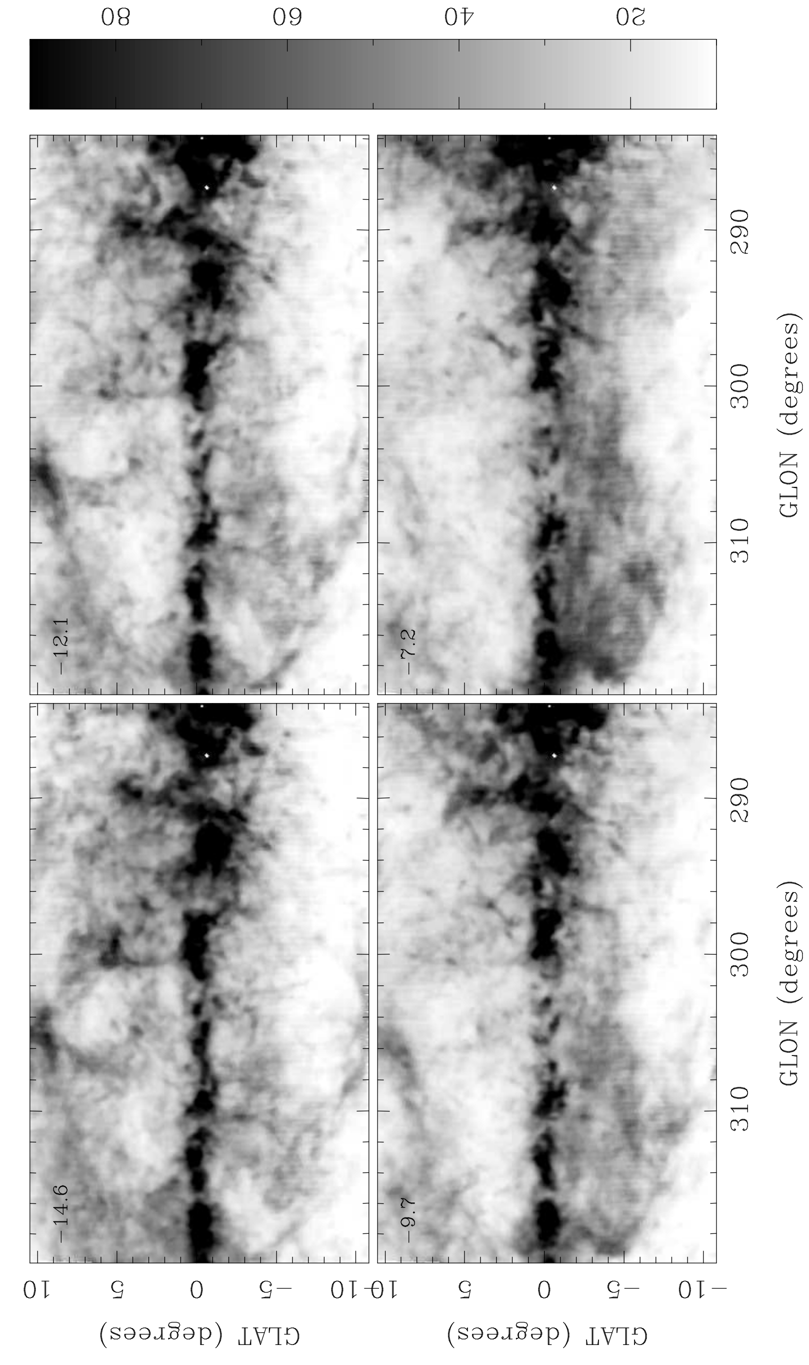

Figure 4.1: Four velocity images of the largest shell, GSH 304+00-12, behind the Coalsack. The images show velocity planes from -7.2 km s^{-1} to -14.8 km s^{-1} and are separated by 2.5 km s^{-1}. The grey scale is linear from 10 - 90 K, as shown in the wedge to the right of the image. The shell, centered at $l = 303\overset{\circ}{.}9$ and $b = -0\overset{\circ}{.}2$, extends to $b = \pm 10\overset{\circ}{.}5$ at the center and is best seen as the arcs above and below the plane on the left of the images.

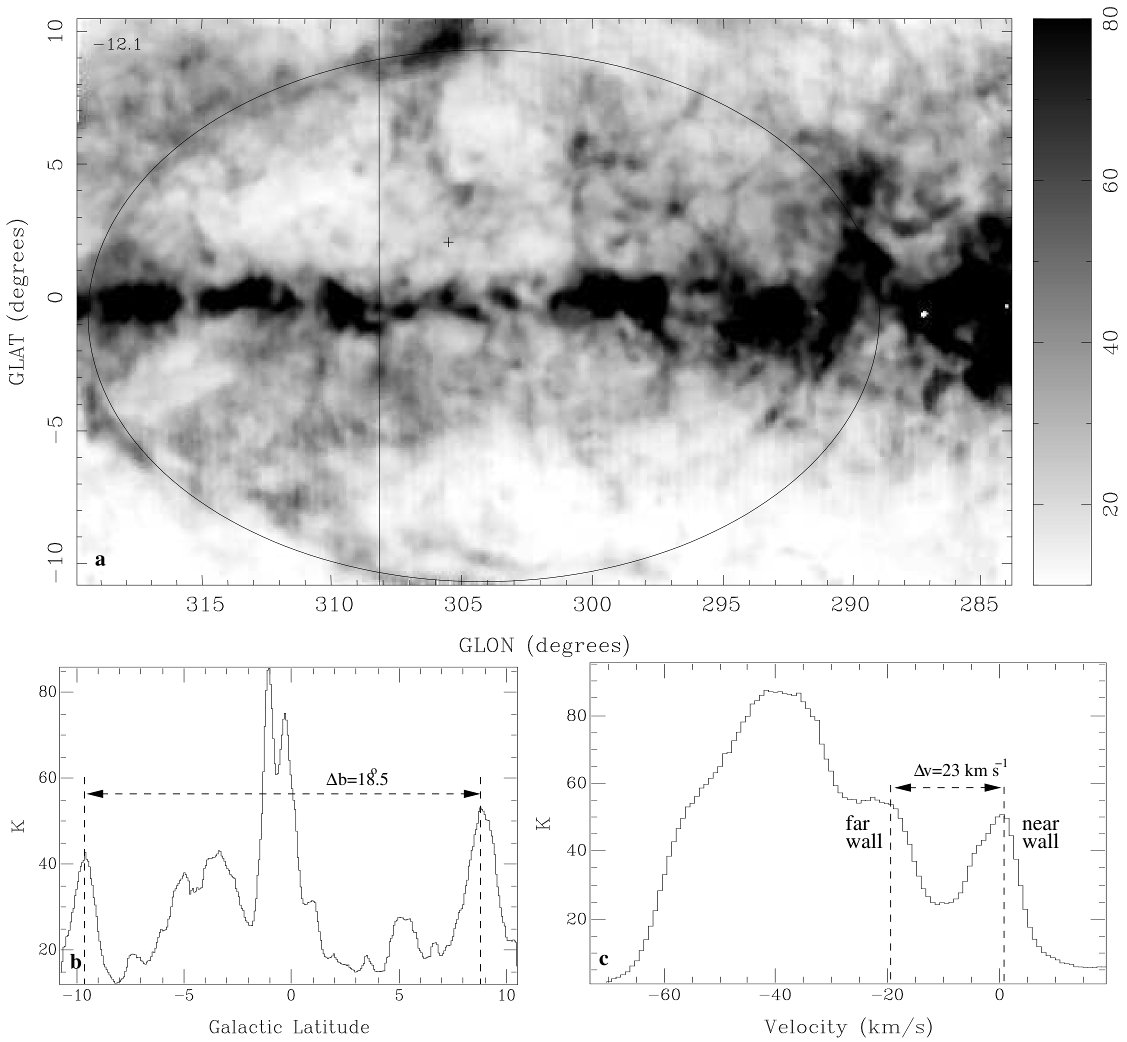

Figure 4.2: H I channel image at $v = -12.1$ km s^{-1} of GSH 304+00-12 (**a**), latitude slice at $l = 308^\circ\!.15$ across the shell (**b**), and a velocity profile through the shell at $l = 305^\circ\!.43$, $b = +2^\circ\!.07$ (**c**). The outline of the shell is marked with the black ellipse on the H I channel image. The vertical line marks the position of the latitude cut (panel **b**) and the cross marks the position of the velocity profile (panel **c**).

and latitude directions, respectively. The near edge of the Sagittarius-Carina arm is at 1.26 ± 0.23 kpc (Seidensticker & Schmidt-Kaler 1989). Although the shell distance errors are large, the coincidence of the shell and spiral arm distances suggests that the shell is at the edge of the arm.

GSH 304-00-12 has a velocity full width of $\Delta v = 23$ km s^{-1}. Disentangling the spatial extent of the shell from the physical expansion is difficult. Because of Galactic rotation, structures that span hundreds of parsecs will be observed over a range of radial velocities, even if they are not expanding. The velocity-distance relationship can be partially separated by considering the velocity gradient along the line of sight. At the location of shell the velocity gradient is ~ 11 km s^{-1} kpc^{-1}. Therefore, if the shell is roughly spherical, such that the shell diameter along the line of sight is on the order of 240 pc, it should extend over approximately 3 km s^{-1} in velocity space. Given the errors involved in deriving distances from the rotation curve, we believe that the velocity expanse due to the shell's physical extent in negligible. Therefore, we estimate the shell's expansion velocity as half of the velocity full width, $v_{\rm exp} \approx \Delta v/2 = 12$ km s^{-1}. This expansion velocity is comparable to shells of similar size in the SMC and somewhat smaller than shells in the LMC (Kim 1998; Stanimirović 1999).

The second shell, GSH 305+01-24, has a smaller angular size of $7^\circ \times 11\overset{\circ}{.}3$ and is located at $l = 305\overset{\circ}{.}1$, $b = +1^\circ$, $v = -24$ km s^{-1}. This shell is centered slightly above the plane and expands further above and below the plane than it does along the plane. An H I image of GSH 305+01-24 at $v = -24$ km s^{-1} is shown in Fig. 4.3 overlaid with the positions of stars in the Cen OB1 stellar association. The relationship of the shell to the stellar association is discussed below.

Like the first shell, GSH 305+01-24 does not have a clearly defined near cap. It does, however, seem to have a far cap. This shell appears to open conically from within the spiral arm at $v \sim -34$ km s^{-1}. It increases in angular size towards larger velocities in the interarm region and reaches its maximum size at $v = -24$ km s^{-1}. The angular size

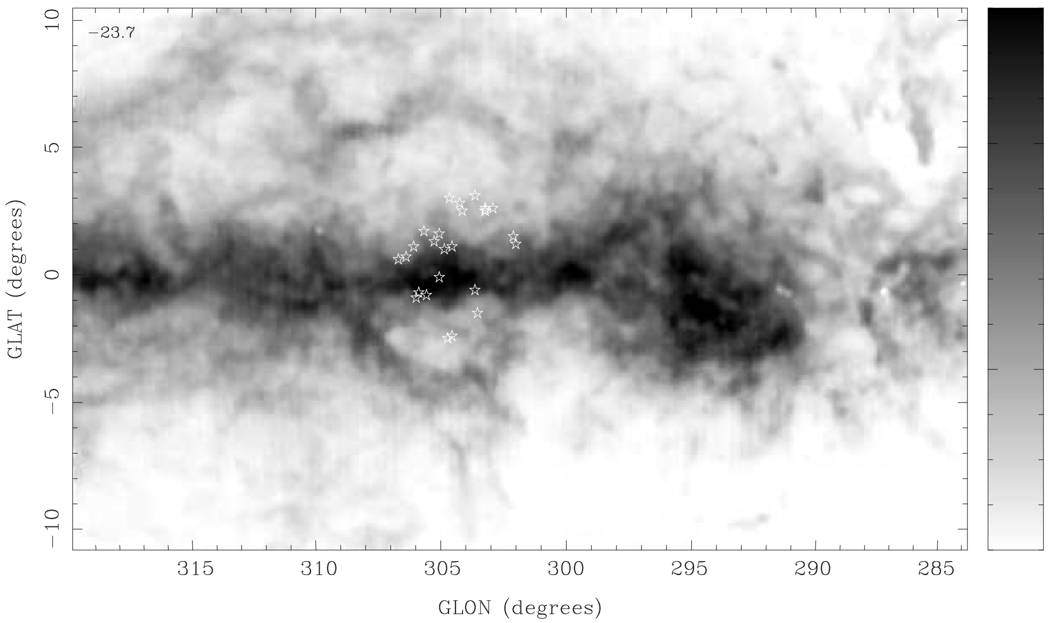

Figure 4.3: H I channel image at $v = -24$ km s^{-1} of GSH 305+01-24 in the edge of the Sagittarius-Carina arm. The grey scale is linear from 10 to 130 K, as shown in the wedge at the right. The shell, of angular diameter $7° \times 11.°3$, is centered at $l = 305.°1$, $b = +1.°0$. The stars mark the positions of stars in the Cen OB1 association (Humphreys 1978).

is relatively constant until $v \approx -20$ km s^{-1}, where the shell begins to close. Beyond $v \approx -20$ km s^{-1}, emission from the shell is confused with that of GSH 304-00-12. The central velocity of $v = -24$ km s^{-1} implies a distance of $D = 2.2 \pm 0.9$ kpc. At this distance the shell has physical radii of 140×220 pc ($l \times b$). GSH 305+01-24 has a velocity full width of $\Delta v = 14$ km s^{-1}. Again, the velocity width due to the physical extent of this shell along the line of sight is probably negligible so we calculate an expansion velocity of $v_{\rm exp} \sim 7$ km s^{-1}.

4.2.1 System Geometry

The ISM along this line of sight is complicated. Spectro-photometric mapping of the region show that the Coalsack nebula is at an average distance of 199 ± 40 pc and consists of at least two overlapping clouds at 188 and 243 pc (Seidensticker & Schmidt-Kaler 1989). CO emission from the Coalsack nebula is geometrically centered at $l = 303°$, $b = 0°$, covers ~ 30 deg^2 on the sky and extends over at least the systemic velocity range $v_{rad} = -10$ to $+8$ km s^{-1} (Bronfman et al. 1989). H I self-absorption from gas in the Coalsack was detected by Bowers et al. (1980) and is also observed in the SGPS dataset. The interarm region between the Coalsack and the edge of the Sgr-Car arm is nearly devoid of dust and molecular gas and the near edge of the spiral arm is at about 1.3 kpc (Seidensticker & Schmidt-Kaler 1989). H I and CO emission between $l = 290° - 320°$ and covering LSR velocities between ~ -40 and ~ -20 km s^{-1} corresponds to the Sgr-Car arm at a mean distance of ~ 2 kpc. For velocities in the range $v \approx -30$ km s^{-1} to $v \approx -18$ km s^{-1} the spiral arm is nearly perpendicular to the line of sight. There is a very slight velocity gradient, such that the high longitude end of the arm is at more negative velocities than the low longitude end.

For a small range of velocities ($-27 \leq v \leq -20$ km s^{-1}) GSH 305+01-24 overlaps with GSH 304-00-12. Though the shells are coincident in velocity space, there is no reason to believe that they are physically overlapping. The central velocities place the shells more than a kiloparsec apart and the line of sight widths are insufficient to overlap the shells. Also, the morphology of the shells do not appear altered by an interaction. The overlap is most likely due to the expansion of the shells and not a true interaction.

Both shells appear to have formed in the edge of the Sagittarius-Carina arm. GSH 305+01-24 seems to close near the edge of the spiral arm, whereas GSH 304-00-12 expands into the interarm region. We suggest that GSH 304-00-12 experienced exaggerated expansion into the interarm region due to the pressure gradient leading away edge of the spiral arm. This explains the relatively constant size over the range of velocities covering the interarm region and the lack of a detectable near cap. GSH 305-00-12 also extends into the range of velocities covered by the Coalsack nebula. The nebula at a distance of 199 ± 40 pc (Seidensticker & Schmidt-Kaler 1989), however, is considerably closer than GSH 304-00-12. Unless the distance to GSH 304-00-12 has been significantly over-estimated or the shell's diameter along the line of sight far exceeds its diameter in the plane of the sky, it is unlikely that the shell is physically interacting with the Coalsack. The lack of emission from a near cap, though, could alternately be explained by absorption by cold H I in the Coalsack.

4.2.2 Related Structures

The lower portion of GSH 305+01-24 was previously identified as an H I shell associated with the Wolf-Rayet star θ Muscae (Cappa De Nicolau & Niemela 1984). However, given the larger field of view in the current observations, this shell arc appears connected with the arc above the plane. The void of GSH 305+01-24 is bisected by emission from the Galactic plane. Because the rotation curve is dual-valued at these velocities, some emission is likely due to much more distant gas located on the far side of the tangent point. In the context of these measurements the θ Muscae shell must be part of the larger structure that we identify as GSH 305+01-24. Cappa De Nicolau & Niemela (1984) also noted a second H I depression at $v = -12$ km s^{-1} that we identify as part of GSH 304-00-12.

There is 2.4 GHz continuum emission corresponding to the lower half of GSH 305+01-24. Fig. 4.4 is a 2.4 GHz continuum image from the Duncan et al. (1995b) survey of the Southern Galactic Plane overlaid with contours of an H I channel image of the shell at $v = -24$ km s^{-1}. The continuum emission excellently traces the inside edge of the shell below the plane. Also, the continuum may trace a portion of the shell above the plane near $l = 301°$, though this emission is very weak making a definitive detection difficult. There is an arc of continuum emission through the upper H I void that does not correspond to any H I features. These arcs were identified by Duncan et al. (1995b) as a possible supernova remnant, G303.5+0. However, close examination of IRAS[1] 100 μm images of the region reveals a very faint infrared shell coincident with the radio continuum features. These features were also identified as an Hα shell, the Coalsack Loop, by Walker & Zealey (1998). The detection of the arcs in the infrared implies that the emission is thermal and therefore suggests that the arcs are not part of a supernova remnant. The close morphological similarity of the lower arcs and the H I shell leaves little doubt that the two are associated. We point out that the Coalsack Loop is much larger in angular size than the Coalsack nebula so that even though the Loop is behind the nebula, extinction in the nebula will not affect the Hα emission. We believe, therefore, that the continuum emission is the photo-ionized region interior to the H I shell.

4.2.3 Is GSH 305+01-24 Associated with Centaurus OB1?

The Cen OB1 stellar association is centered at $l = 304°$, $b = +0.^{\circ}5$ with radial velocities in the range -38 km s^{-1} to -10 km s^{-1}. The adopted distance is 2.5 kpc (Humphreys 1978), which puts the cluster, to within the errors, at the same distance as GSH 305+01-24. The positions of the stars are plotted on a channel image of GSH 305+01-24 at $v = -22$ km s^{-1} in Fig. 4.3. The morphology of the shell appears to trace the stellar distribution, suggesting an association. The shell extends further above the plane than below, a characteristic that is matched by the stellar distribution. The cluster contains 21 stars with measured luminosities and temperatures and calculated ages and masses (Humphreys 1978; Kaltcheva & Georgiev 1994). The earliest stars in the association are of type O9, which suggests that more massive stars may have already exploded as supernovae. A Wolf-Rayet star, θ Muscae, of spectral type WC6 is also in the cluster. This system is a binary, possibly a triple, consisting of the W-R+O close binary and a distant O supergiant (Hartkopf et al. 1999). A priori, it seems likely that this association

[1] See IRAS Sky Survey Atlas Explanatory Supplement at http://www.ipac.caltech.edu/ipac/iras/issa.html

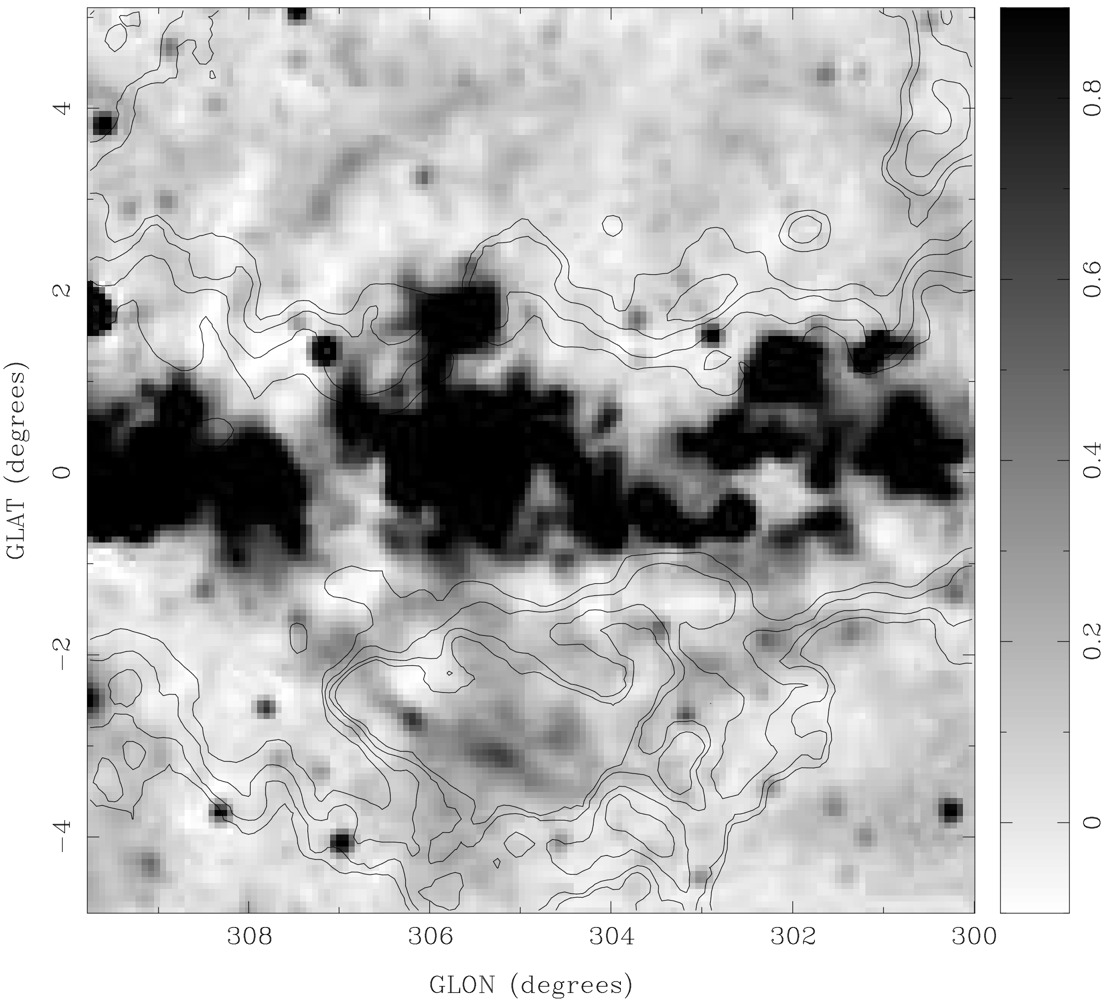

Figure 4.4: Grey scale image of the 2.4 GHz continuum emission of the GSH 305+01-24 region overlaid with H I contours at $v = -24$ km s^{-1}. The grey scale is linear and goes from 0.1 to 0.9 mJy Bm^{-1} as shown in the wedge at the right. The continuum image is from the Duncan et al. (1995b) survey of the Galactic Plane and has been filtered to enhance small scale structure as described therein. The H I contours are at 45, 50, 60, and 70 K of T_b. The faint arcs of continuum emission in the lower half of GSH 305+01-24 trace the interior edge H I shown as shown by the contours.

is the energy source for the GSH 305+01-24.

To explore whether GSH 305+01-24 could be explained as a wind-driven bubble associated with Cen OB1, we employed a very simple one-dimensional numerical model to study the evolution of a shell powered by the stars in this association. The model follows standard equations for the evolution of a pressure-driven wind bubble (e.g. Weaver et al. 1977; Oey & Massey 1995). The system is simplified to contain a centrally located power source, in this case the OB association, that supplies a time-dependent wind luminosity which drives the expansion of a shell. We assume that the internal pressure and temperature are constant throughout the bubble interior. The system is further simplified by assuming an ideal, monatomic gas equation of state, and a cool, homogeneous external medium. The bubble expansion can be described by three first-order equations: the rate of expansion of the shell, the equation of momentum conservation and the equation of energy conservation. The rate of expansion, $v_{\rm exp}$, is simply the first-derivative of the shell radius, R_{sh},

$$\frac{dR_{sh}}{dt} = v_{\rm exp}. \tag{4.1}$$

The momentum conservation equation, including the effects of external and internal pressure, P_e and P_i, respectively, is

$$\frac{dv_{sh}}{dt} = \frac{4\pi R_{sh}^2}{M_s}\left(P_i - P_e - \rho_e v_{\rm exp}^2\right), \tag{4.2}$$

where M_s is the mass of the shell and ρ_e is the density of the ambient medium. The equation of energy conservation is

$$\frac{dE_{sh}}{dt} = L_w - P_i\frac{dV}{dt}, \tag{4.3}$$

where L_w is the wind luminosity and V is the bubble volume, $V = (4\pi/3)R_{sh}^3$. The internal energy of the shell, E_{sh}, is related to the internal pressure according to the relation

$$E_{sh} = \frac{P_i V}{\gamma - 1}, \tag{4.4}$$

where the adiabatic index is $\gamma = 5/3$. The wind luminosity, $L_w = 1/2\dot{M}v_\infty^2$, is calculated from an estimate of the mass-loss rate, $\dot{M}$, and escape velocity, v_∞, of each star in the Cen OB1 association. The external pressure is given by $P_e = \rho_e c_s^2 \gamma^{-1}$, where c_s is the local speed of sound in the external medium, which is assumed to be ~ 10 km s^{-1} for a warm neutral medium at $T \sim 5000$ K. Using temperatures, luminosities, masses, and ages for 21 Cen OB1 stars tabulated by Kaltcheva & Georgiev (1994), we estimate the mass-loss rate from the empirically determined mass-loss rates of OB stars made by de Jager et al. (1988). The terminal velocity is estimated from the OB stellar wind model of Leitherer et al. (1992). Using the ages of the stars we calculate the total wind luminosity as the sum of all stars that exist at each time step. Only stars for which masses, luminosities, and ages are available are included in the model. The spectral type, escape velocities, mass-loss rates, and wind luminosities are given in Table 4.1. For simplicity, we assume a constant external density, $\rho_e = 1.67 \times 10^{-24}$ gm cm^{-3}, corresponding to one hydrogen atom per cubic centimeter. The model is calculated with time steps of 1.5×10^3 yr and the initial conditions are calculated from the self-similar solutions to the differential equations at the first time step, $t = 1.5 \times 10^3$ yr.

The results of the numerical integration are shown in Fig. 4.5. We explored two cases: one where the luminosity increases with time as stars are "born" in the association and another case of constant luminosity equal to the sum of all stars, regardless of age. The time-dependent wind luminosity case is plotted with a solid line and the constant wind luminosity case is plotted with a dashed line. The vertical dotted line marks the age of the oldest star in the association (14.7 Myr), with time $t = 0$ assumed to be the birth of that star. The expansion velocity flattens near 14 Myr because of the high mass-loss rate of the Wolf-Rayet star, θ Muscae. Several differences between the two models are of note. First, the shell radius for the constant wind luminosity case can be fit as $R_{\rm sh} \propto t^{3/5}$, the analytic self-similar solution to the problem. But, in the time-dependent wind luminosity case the radius goes as $t^{3/5}$ initially and then is

Table 4.1: Properties of massive stars in the Cen OB1 stellar association included in the numerical model for GSH 305+01-24.

Star	Spectral Type[a]	Age (Myr)	v_∞ (km s^{-1})	Log $\dot{M}$ ($M_\odot$ yr^{-1})	L_w (10^{35} erg s^{-1})	E_{tot}[b] (10^{49} erg)
HD 110639	B1 Ib	10.3	1514.1	-6.22	4.35	14.15
HD 111613	A2 Iab	11.9	893.8	-6.10	2.00	7.51
HD 111904	B9 Ia	9.6	979.5	-5.30	15.15	45.91
HD 111934	B2 Ib	9.1	1427.3	-5.60	16.13	46.31
HD 111973	B5 Ia	8.6	1169.3	-5.91	5.30	14.39
HD 111990	B3 Ib	11.0	1341.4	-5.40	22.58	78.37
HD 112272	B0.5 Ia	4.7	1563.9	-5.52	23.28	34.52
HD 112366	B9 Ia-Ia	10.0	1044.1	-5.40	13.68	43.16
HD 112364	B0.5 Ib	12.0	1607.1	-5.90	10.25	38.81
HD 112842	B3 Ib	14.7	1201.5	-5.40	18.11	84.02
HD 113012	B0 Ib	12.6	1764.2	-6.22	5.91	23.50
HD 113422	B1 Ia	6.5	1423.9	-5.92	7.68	15.75
HD 114011	B1 Ib	12.9	1637.7	-6.14	6.12	24.92
HD 114213	B1 Ib	9.5	1320.5	-6.22	3.31	9.93
HD 115704	B0.5 Ia-Iab	3.7	1568.0	-6.15	5.49	6.40
HD 116119	A0 Ia	10.2	1006.3	-7.16	0.22	0.71
HD 115363	B1 Ia	3.6	1494.8	-5.27	37.82	42.96
HD 114122	B0.5 Ia-Iab	7.6	1560.5	-6.15	5.43	13.03
HD 114886	O9 II-III	4.9	2161.6	-5.57	39.64	61.29
HD 113421	B0.5 III	6.7	2386.8	-6.90	2.26	4.78
HD 113708	B0.5 III	6.2	2197.7	-6.90	1.92	3.75
WR 48[c]	WC6+O9.5I	···	2000.0	-3.74	2294.0	217.17

[a]From Humphreys (1978).

[b]Total lifetime energy input, $E_{tot} = L_w t$, where t = age

[c]The W-R+O9.5 close binary is assumed to exist in its current state of high mass loss for $\sim 3\times10^5$ yr. The mass loss rate and terminal velocity are from Leitherer et al. (1997).

Note: Only stars with observed temperatures, luminosities, masses and ages were used. Terminal velocities were estimated from the OB stellar wind model ofLeitherer et al. (1992). The mass-loss rates are based on the empirically determined mass-loss rates of OB stars in de Jager et al. (1988). In the model, stars are 'turned on' at 14.7 Myr minus their age.

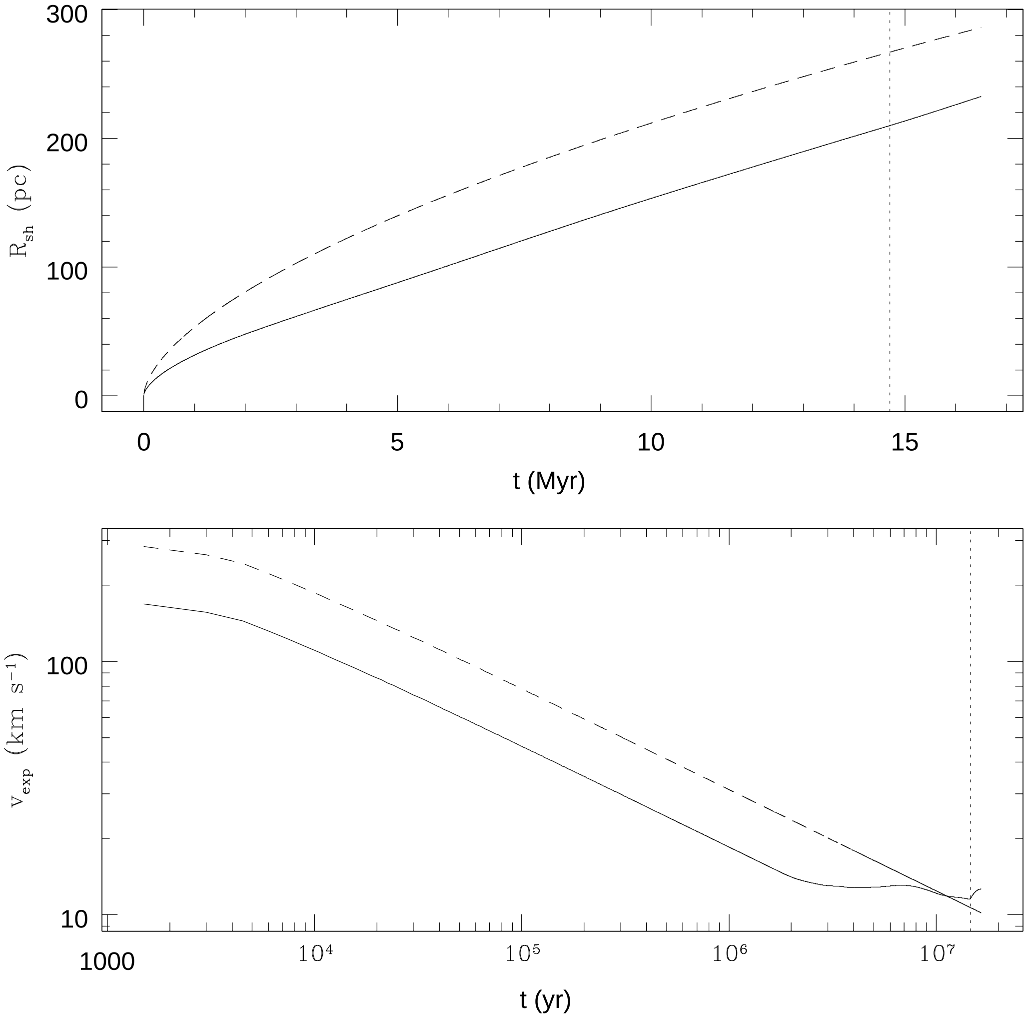

Figure 4.5: Simple numerical model of the shell radius and velocity evolution calculated for a constant luminosity input equal to the sum of the Cen OB1 stellar wind luminosities (dashed line) and for a time dependent total wind luminosity calculated from the ages, masses and luminosities of the Cen OB1 population (solid line). The vertical dotted line marks the present age of the stellar association. The actual shell radius and expansion velocity are well modeled by a time-dependent wind luminosity. The flattening of the velocity curve near 14 Myr in the time dependent model is due to the Wolf-Rayet star.

better fit as $R_{sh} \propto t$. Second, the usual assumption of coeval star formation for stellar associations leads to a slight over-estimate of the total energy input in a wind blown bubble. This effect is most noticeable as an overall increase in final shell radius by a factor of ~ 1.4; expansion velocity is relatively insensitive to the total energy input for larger ages. It seems, then, that including the stellar ages in the wind luminosity model results a marginally better fit to the data.

We find that GSH 305+01-24 is surprisingly well described by the Weaver et al. (1977) model of a wind-blown bubble with a time-dependent wind luminosity from Cen OB1 stars. This model predicts a shell radius of ~ 210 pc, which corresponds well with the measured radii of 140×220 pc; whereas the time-independent luminosity model predicts a radius of ~ 300 pc. The model predicts an expansion velocity of ~ 11 km s^{-1} for both the time independent and dependent luminosity cases, which also agrees well with an inferred expansion velocity of ~ 7 km s^{-1}. The good agreement suggests that GSH 305+01-24 was indeed formed from the stellar winds of the Cen OB1 association. The size and expansion velocity are consistent with a shell age approximately equal to the age of the oldest star in the association (~ 15 Myr). Kaltcheva & Georgiev (1994), however, derive an age of 8.9 ± 3.1 Myr for Cen OB1, from the average of the population's ages. The stellar ages are evenly distributed from 14.7 Myr to 3.6 Myr with no evidence for sequential star formation, but rather there is evidence for continuous star formation, which makes it difficult to define an age for the cluster. Using the wind luminosities and ages of the Cen OB1 association stars we find the total energy released in the form of stellar wind luminosity during the lifetime of the association is $\sim 8.3 \times 10^{51}$ ergs. We can compare this to the expansion energy of the shell - the equivalent energy instantaneously deposited at the center of the shell - derived by Chevalier (1974) and given in equation 2 of Heiles (1979): $E_E = 5.3 \times 10^{43}\, n_0^{1.12}\, v_{\rm exp}^{1.4}\, R_{sh}^{3.12}$. To account for the current radius and rate of expansion of GSH 305+01-24, the expansion energy is $\sim 9.8 \times 10^{51}$ ergs, which agrees well with the total energy of the Cen OB1 stellar winds.

Limitations of the Model

The model shows, as it was intended to do, that the origin of GSH 305+01-24 can be explained, with respect to the energetics, as stellar wind luminosity from the Cen OB1 association. Despite the good reproduction of the shell characteristics by this model, it should be stressed that it is a over-simplification and cannot replace full magnetohydrodynamical simulations of H I shells from OB associations. No attempts have been made to include multi-dimensional modeling, radiative cooling, magnetic fields, or the spatial distribution of the energy input sources. Additionally, the model contains no morphological information that can be helpful when trying to fully understand shell dynamics. Here we summarize some of the components of a non-idealized ISM that have not been included in the calculations and how those might effect the results.

The model neglects energy injection from supernovae because there is no direct evidence for any associated with this cluster. However, it is possible that there have been supernovae in the association. The effect of supernovae on the wind-driven bubble evolution is very similar to that of stellar winds as an input energy source (McCray & Kafatos 1987; Chu & Mac Low 1990). McCray & Kafatos (1987) show in their equation 1 that for a standard initial mass function, an association of $N_\star$ stars with mass greater than 7 $M_\odot$, supernovae input a mean luminosity over the association lifetime of $P \approx 6.3 \times 10^{35}(N_\star E_{51})$ ergs^{-1}. However, only $\sim 20\%$ is available in the first 10 Myr. Therefore, if $N_\star \sim 15$, supernovae would have increased the modeled radius and expansion velocity of GSH 305+01-24 by about a factor of two.

As shown in Fig. 4.3 the stars of the Cen OB1 association are distributed throughout the interior of GSH 305+01-24. The model, however, assumes all stars are at the center of the shell. The B stars may have migrated as much as $\sim$ 50 pc in the shell lifetime (McCray & Kafatos 1987), which suggests that the stars could have been initially distributed over a region $\lesssim$ 100 pc in diameter. This inferred remaining distribution should be negligible on the calculated shell radius and expansion velocity, but could affect the morphology of the shell.

The shell morphology would likely be dominated by external density variations that were not included in this model. As shown in studies of supershell expansion in stratified media (e.g. Mac Low et al. 1989), shells expanding out of the plane of the Galaxy experience exaggerated expansion and blow-outs in that direction. For GSH 305+01-24, the shell radius is on the order of the scale height of the H I disk, at which height the density gradient of the disk becomes significant. Also, as noted above, the shells are at the edge of the Sagittarius-Carina spiral arm, so the density and pressure should decrease into the interarm region. Both of these effects will undoubtedly lead to exaggerated expansion down both density gradients. Small scale density fluctuations and the development of instabilities in the course of shell expansion can also effect the shell shape and size and can lead to break-outs in localized regions. The effect of such break-outs would be to equalize the internal and external pressures and stall expansion.

Finally, three dimensional simulations of shell expansion in multi-phased, magnetized, turbulent media show shells that are far from circular and exhibit many merging cavities and tunnels rather than a fully empty void (Korpi et al. 1999). Uniform magnetic fields in the disk can act to temporarily confine shells to the plane, and thereby affect the shell radius (Tomisaka 1998). Clearly, the model employed here has numerous limitations, but it adequately shows that winds from the Cen OB 1 association can account for the observed shell radius and expansion velocity.

4.3 Conclusions

We have shown images of two new H I shells, GSH 305+01-24 and GSH 304+00-12, located at the edge of the Sagittarius-Carina spiral arm in the direction of the Coalsack nebula. Both shells are very large, with radii on the order of 200 pc. We employed a simple time dependent wind luminosity model based on the ages and luminosities of the stars in the Cen OB1 association to describe the evolution of GSH 305+01-24. The model predictions agree well with the observed shell radius and expansion velocity. We use this agreement, the positional coincidence of the shell and OB association, and the similarities between the shell morphology and the stellar distribution to argue that GSH 305+01-24 is a wind-blown bubble. This shell is associated with a 2.4 GHz radio, infrared and Hα continuum shell that were previously posited to be an old supernova remnant (Duncan et al. 1995b; Walker & Zealey 1998). Because of the infrared detection of the shell we believe that the emission is thermal and therefore not part of a supernova remnant, but instead emission from the shell itself.

We also found a large angular diameter shell, GSH 304-00-12, that does not appear to have formed from any known stellar associations. This shell is embedded in the edge of the Sagittarius-Carina arm and expanded into the interarm region, resulting in a conical geometry. We find no corresponding emission features in other wavebands. GSH 304-00-12 has no detectable near cap, but the velocities where the cap is expected overlap velocities in the Coalsack nebula. We believe that there is no physical association between the nebula and the shell, but we suggest that emission from the cap may be absorbed by cold H I in the nebula. Additionally, although GSH 305+01-24 and GSH 304-00-12 overlap in velocity space, there is no direct evidence for any interaction between them.

Acknowledgments
N. M. M.-G. would like to thank E. J. Hallman for helpful conversations and code. We would also like to thank the anonymous referee for helpful suggestions that improved the paper. J. M. D. and N. M. M.-G. acknowledge support of NSF grant AST-9732695 to the University of Minnesota. N. M. M.-G. is supported by NASA Graduate Student Researchers Program (GSRP) Fellowship NGT 5-50250. B. M. G. acknowledges the support of NASA through Hubble Fellowship grant HST-HF-01107.01-A awarded by STScI, which is operated by AURA Inc. for NASA under contract NAS 5-26555.